

# Composite least mean fourth algorithm (CLMF) based dynamic voltage restorer for enhancement of power quality

Tummala Kranti Kiran<sup>1</sup>, Balakrishnan Rajagopal<sup>1</sup>, Yerramilli Butchi Raju<sup>2</sup>

<sup>1</sup>Department of Electrical Engineering, Annamalai University, Tamil Nadu, India

<sup>2</sup>Department of Electrical and Electronics Engineering, Sir C. R. Reddy College of Engineering, Andhra Pradesh, India

## Article Info

### Article history:

Received Sep 13, 2024

Revised May 10, 2025

Accepted Jul 23, 2025

### Keywords:

Adaptive filtering control  
Composite least mean fourth  
Dynamic voltage restorer  
Harmonic compensation  
Power quality

## ABSTRACT

This paper introduces the composite least mean fourth control algorithm (CLMF) with a dynamic voltage restorer (DVR) to address power quality problems linked to voltage at the source side and supply clean voltage to the distribution network's sensitive loads. The performance of the two least mean fourth adaptive filters combined convexly by this control technique is better than that of the filters working independently. When comparing the suggested control to conventional synchronous reference frame-based vector control, phase-locked loops, abc to dq transformations, and dq to abc transformations are all practically eliminated. When compared to standard least mean square (LMS) and least mean fourth (LMF) control approaches, the proposed CLMF's features—simple computation, ease of implementation, reduced settling time, and increased reliability—show that the suggested controller is more efficient. The proposed CLMF controller excels in terms of rise time, 0.082 sec., and less settling time, 0.092 sec., respectively, with a peak overshoot of 2.33% compared with the aforementioned control algorithms. Different voltage-related PQ issues have been corrected successfully by the proposed CLMF. Through simulation using MATLAB/Simulink, system performance has been verified.

*This is an open access article under the [CC BY-SA](#) license.*



## Corresponding Author:

Tummala Kranti Kiran  
Department of Electrical Engineering, Annamalai University  
Annamalainagar, Tamil Nadu 608002, India  
Email: krantikiran.tummala@gmail.com

## 1. INTRODUCTION

Electrical power fluctuations (flickers) can cause disruptions to several vital systems used in homes, hospitals, industries, cellular network base stations, and the IT industry. The power grid usually experiences harmonic distortions, voltage swell, and voltage sag (voltage dip) as a result of these changes [1]-[3]. According to several statistical studies [4], [5], voltage sag is a frequent voltage disturbance problem that has a negative impact on production costs. Possible reasons for voltage sag/swell include energizing big motors or transformers, switching activities, defects (short circuits), and sudden changes in load [6]. Dynamic voltage restorers (DVRs) are widely used in the industrial sector and are one of the most effective ways to reduce distortions, imbalance, and voltage sag and swell [7]. The overall performance and transient adaptability of the DVR system are critical in supplying sensitive equipment linked with high-quality power. On DVR structure, algorithms for control, and modes of operation, a large body of literature exists.

A dynamic voltage restorer (DVR) that may lessen voltage sag in power systems can be controlled using a unique dual-slope delta modulation (DSDM) technology, as demonstrated in [8]. For the purpose of restoring the load voltage to its nominal value, this approach creates switching pulses for the CSI's power electronic switches, which in turn provide the necessary phase angle jumps and missing voltage waveforms.

A separate PWM pulse generator and a phase-locked loop (PLL)-based artificial neural network (ANN) controller are employed in [9] for DVR control. A BES-based DC-DVR that mitigates the adverse impact of voltage sag/swell occurrences on delicate loads in the DC network is described in [10]. Preview study [11], a dynamic voltage restorer (DVR) application employs the frequency feedback loop-based cascade delayed signal cancellation PLL to counteract grid voltage disruptions. The DVR system is controlled by the decoupled  $\alpha\beta$ -PLL, which is provided [12]. This controller coupled a closed-loop feedback control signal with a feedforward control signal. A solar energy-based single-phase DVR with a fuzzy logic-controlled innovative boost inverter was used to reduce deep voltage sags, swells, and interruptions [13]. Researcher in [14] suggests a super-twisting sliding mode control technique for single-phase three-level T-type inverter-based dynamic voltage restorers. DVR employs an intricate wavelet transform-based control technique to identify and address voltage-related PQ issues [15]. The ESRF theory-based DVR is used in [16] to keep the ASD's DC-link voltage at its reference value during the sag period, which causes the motor to run at a constant speed.

It has been demonstrated that the theory of adaptive filters is capable of monitoring changes in the surroundings and characteristics of unidentified systems where the filter is employed. As conditions change, the filter variables self-tune, maintaining the environment's and the filter system's behavior to fulfil their intended roles. Three types of control have been established to capture the phase angle and number of harmonics in a power system: LMS-based control, least mean fourth (LMF), and least mean square/fourth (LMS/F) based control [17]. The D-STATCOM with the LMF control method is implemented in [18]. The distributed static compensator used in [19] generates the active and reactive components by combining LMS and LMF. The new control algorithms, such as variable step-size Griffith's LMS [20] and variable learning factor least mean square algorithm [21], have been implemented for DVR operation. The adaptive filter algorithm family includes the LMF technique. Walach and Widrow [22] modified the least mean square (LMS) algorithm in 1984 and created the least mean fourth (LMF) method. The LMF approach has substantially less noise in the weights than the traditional LMS algorithm when the time constant values for the two approaches are equivalent. The main goal of the LMF algorithm is to create a restricted steady state of maladjustment for the specified learning rate, which is different from the LMS approach. The LMS approach cannot attain high steady-state performance in situations with low signal-to-noise ratios (SNRs) because it functions as a lower-order adaptive filter. In order to overcome this difficulty and improve the system's steady-state performance, a fourth-order power optimization has been put into place [23]. Even in areas with poor SNR, noise interruptions can be neutralized by it. Because of this, the LMF approach has a fourth-order power optimization updating equation and operates as a higher-order adaptive filter. It has been demonstrated that adaptive algorithms with high-order moments of errors, such as LMF, outperform traditional LMS algorithms in terms of mean square error (MSE) [24]. An approach to enhance the adaptive theory is to propose a composite of two adaptive transverse filters [25].

Prior to being integrated for the purpose of minimizing errors overall, two filters independently adjust to respective error signals. System dynamic performance is degraded by the sluggish convergence rate of LMF and standard LMS filters. To address these problems, two filters are combined. A convex combination of LMF is used to eliminate the trade-off, and the convex filter always guarantees the best tracking performance. The convex filter gets its name from its ability to always select the highest-performing component filter. Retrieving harmonics from sinusoids using the suggested CLMF-based control technique has never been successfully implemented.

This work proposes a two-filter combination for fast-tracking and accuracy. It is said to be better in the following areas than the current standard algorithms (SRFT, IRPT, and so forth): It is more stable, takes less time to settle, and has been shown to be more reliable than SRFT and IRPT. It encompasses basic computation and is easy to implement because it uses simple mathematical blocks for calculation, whereas SRFT and IRPT use complex blocks like a phase-locked loop (PLL) and so on. The CLMF algorithm is implemented in this work to operate the DVR. The main contributions include:

- The recommended convex combination of the least mean fourth (CLMF) control method employed for DVR operation has an adaptable character and quickly converges to extract the fundamental source voltage (FSV) component.
- The compromise between tracking capabilities and accuracy of LMF filters owing to fixed stepping is addressed by the CLMF algorithm, which provides a combination of two filters for rapid tracking and precision. Furthermore, the suggested controller does not require a sophisticated PLL architecture.
- The suggested controller outperforms traditional LMS and LMF adaptive filters in terms of total harmonic distortions (THD) analysis, computation complexity, steady-state, and dynamic performance.

The outline of the paper includes DVR system configuration, details of the proposed control algorithm, a discussion on results, and the comparison of the proposed control algorithm with previously developed control algorithms.

## 2. SYSTEM CONFIGURATION

Figure 1 shows how the DVR system is designed. It is feasible to attach different kinds of loads at different periods to disrupt the PCC by using a switch or breaker. Voltage sag and swell are experienced by the supply voltage when the inductive and capacitive loads are turned on. Harmonics and voltage imbalance are created in the supply voltage in the same way by turning on the diode rectifier with an RL-load and the three-phase unbalanced load. In order to evaluate real-time performance, supply voltage is obtained at the point of common coupling (PCC) after taking the influence of source impedance into account. The load voltages and load currents are monitored at the load bus, which is linked to the crucial load. The DC bus capacitor is chosen with the ability to respond quickly to dynamic changes in the system under consideration. The control algorithm generates gate pulses that assist the voltage source converter (VSC) in converting DC to AC voltage. The DVR operates in response to a disruption in the system, and it uses the injection transformer and VSC to inject the required voltage into the system. The CLMF control algorithm is responsible for realizing the gating signals to the VSC. As a result, the power quality improves and the load voltage turns sinusoidal.

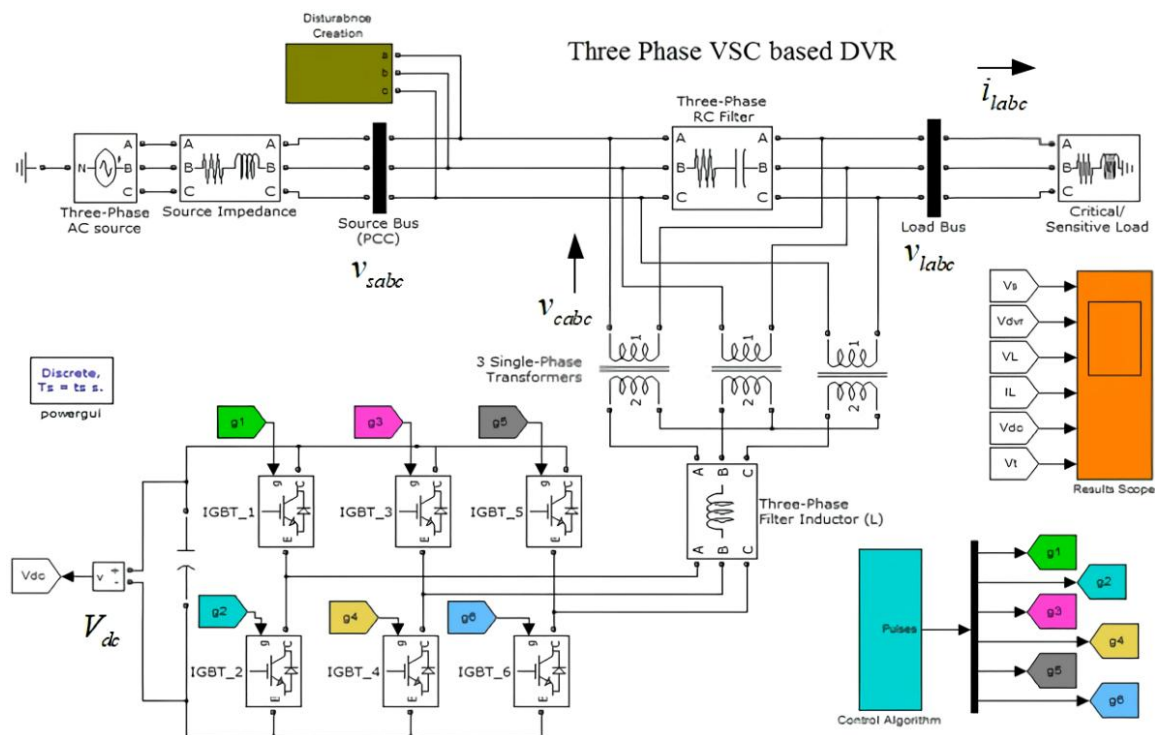


Figure 1. System configuration of DVR: control strategy of DVR using composite least mean fourth (CLMF) algorithm

## 3. CONTROL ALGORITHM

The overall structure of the CLMF control method is shown in Figure 2. A recommended CLMF control algorithm must be used to extract the basic active and/or reactive component from the three supply voltage phases, as shown in Figure 2. The basic active components extraction unit, the reactive component extraction unit, and the PCC voltage amplitude calculation, which may be utilized to produce the load reference voltage, are depicted in this diagram. The active and reactive fundamental components of each phase have been averaged to find the fundamental components of the three-wire supply voltage.

### 3.1. Conversion of line voltage sensed into phase voltage

In the beginning, the line voltages  $v_{ab}$  and  $v_{bc}$  are anticipated at the PCC and phase voltages  $v_{sa}$ ,  $v_{sb}$  and  $v_{sc}$  are computed with the help of the formula as (1)-(3) [24].

$$v_{sa} = \frac{2}{3}v_{ab} + \frac{1}{3}v_{bc} \quad (1)$$

$$v_{sb} = -\frac{1}{3}v_{ab} + \frac{1}{3}v_{bc} \quad (2)$$

$$v_{sc} = -\frac{1}{3}v_{ab} - \frac{2}{3}v_{bc} \quad (3)$$

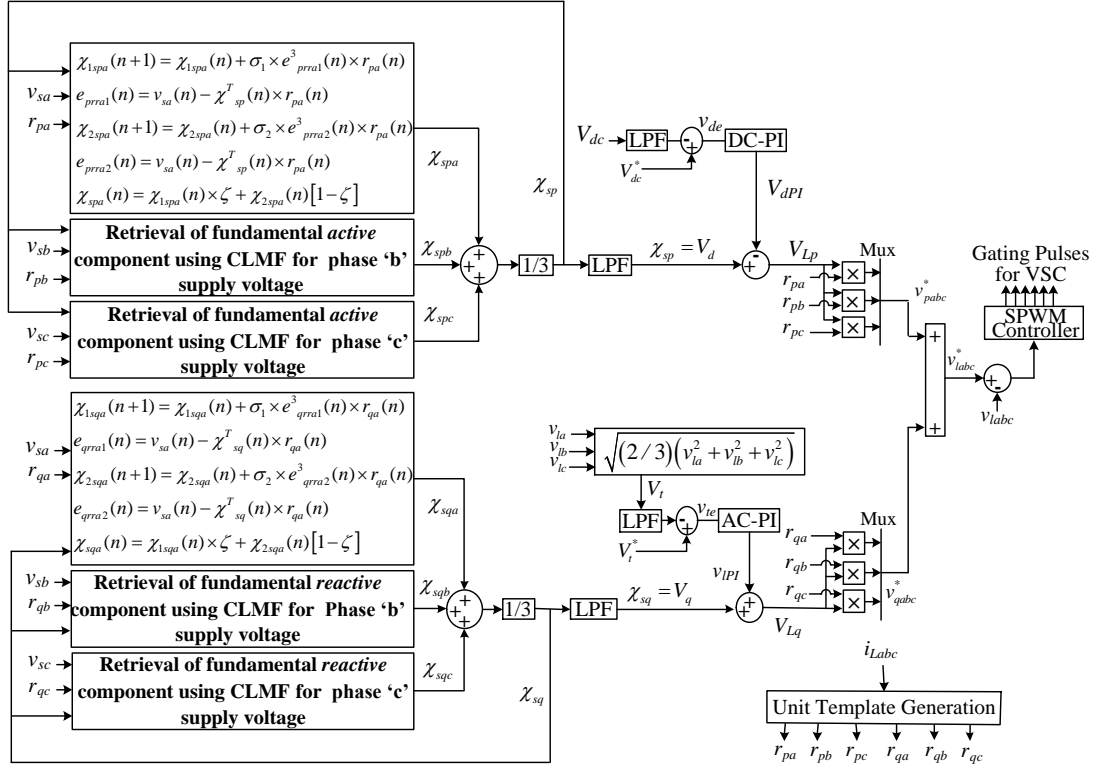


Figure 2. System configuration of DVR: overall CLMF-based control algorithm

### 3.2. Unit template evaluation and terminal load voltage amplitude calculation

The generated load voltages are composed of two components, one of which is in the same phase as the PCC voltage and is known as the in-phase component  $r_{pabc}$ , and the other is in quadrature  $r_{qabc}$  with the PCC voltage. The load current  $i_{Labc}$  is used for the evaluation of unit templates. The peak amplitude of load current  $I_{LA}$  is calculated as (4).

$$I_{LA} = \sqrt{\frac{2}{3}} * \sqrt{\{(i_{La})^2 + (i_{Lb})^2 + (i_{Lc})^2\}} \quad (4)$$

The predicted in-phase unit templates are as (5).

$$r_{pk} = \frac{i_{Lk}}{I_{Lk}}; k = a, b, c \quad (5)$$

Furthermore, the in-phase unit templates are utilized for the prediction of the quadrature unit template as (6).

$$\begin{aligned} r_{qa} &= \frac{(-r_{pb} + r_{pc})}{\sqrt{3}} \\ r_{qb} &= \frac{3r_{pa} + r_{pb} - r_{pc}}{2\sqrt{3}} \\ r_{qc} &= \frac{-3r_{pa} + r_{pb} - r_{pc}}{2\sqrt{3}} \end{aligned} \quad (6)$$

The terminal load voltage amplitude can be calculated as (7).

$$V_t = \sqrt{\frac{2}{3}} * \sqrt{\{(v_{La})^2 + (v_{Lb})^2 + (v_{Lc})^2\}} \quad (7)$$

### 3.3. Retrieval of fundamental active components using the CLMF algorithm

The proposed algorithm uses a convex composition of the LMF. Here, in this work, two LMF adaptive filters have been used. The equations of LMF applied for phase ‘a,’ phase ‘b,’ and phase ‘c’ are identical. The generalized equation of LMF for retrieval of the fundamental active component is as (8).

$$\chi_{ispm}(n+1) = \chi_{ispm}(n) + \sigma_i \times e^3_{prmi}(n) \times r_{pm}(n); m = a, b, c; i = 1, 2 \quad (8)$$

Hence, the weight equation of the first LMF adaptive filter for retrieval of the fundamental active component of phase ‘a,’ phase ‘b,’ and phase ‘c’ can be written as (9).

$$\begin{bmatrix} \chi_{1spa}(n+1) \\ \chi_{1spb}(n+1) \\ \chi_{1spc}(n+1) \end{bmatrix} = \begin{bmatrix} \chi_{1spa}(n) \\ \chi_{1spb}(n) \\ \chi_{1spc}(n) \end{bmatrix} + \sigma_1 \times \begin{bmatrix} e^3_{prra1}(n) \times r_{pa}(n) \\ e^3_{prrb1}(n) \times r_{pb}(n) \\ e^3_{prrc1}(n) \times r_{pc}(n) \end{bmatrix} \quad (9)$$

Where the term  $e_{prra1}(n), e_{prrb1}(n), e_{prrc1}(n)$  shown in (9) is the adaptive component error, which is obtained as (10).

$$\begin{bmatrix} e_{prra1}(n) \\ e_{prrb1}(n) \\ e_{prrc1}(n) \end{bmatrix} = \begin{bmatrix} v_{sa}(n) \\ v_{sb}(n) \\ v_{sc}(n) \end{bmatrix} - \chi^T_{sp}(n) \times \begin{bmatrix} r_{pa}(n) \\ r_{pb}(n) \\ r_{pc}(n) \end{bmatrix} \quad (10)$$

The term  $v_{sa}(n), v_{sb}(n), v_{sc}(n)$  is the phase voltage of the source,  $\chi_{1spa}(n), \chi_{1spb}(n), \chi_{1spc}(n)$  is the weight of the fundamental active component for all three phases of the first filter. The weight component of the second filter, along with its error equations, can be depicted as (11).

$$\begin{aligned} \begin{bmatrix} \chi_{2spa}(n+1) \\ \chi_{2spb}(n+1) \\ \chi_{2spc}(n+1) \end{bmatrix} &= \begin{bmatrix} \chi_{2spa}(n) \\ \chi_{2spb}(n) \\ \chi_{2spc}(n) \end{bmatrix} + \sigma_2 \times \begin{bmatrix} e^3_{prra2}(n) \times r_{pa}(n) \\ e^3_{prrb2}(n) \times r_{pb}(n) \\ e^3_{prrc2}(n) \times r_{pc}(n) \end{bmatrix} \\ \begin{bmatrix} \chi_{2spa}(n+1) \\ \chi_{2spb}(n+1) \\ \chi_{2spc}(n+1) \end{bmatrix} &= \begin{bmatrix} \chi_{2spa}(n) \\ \chi_{2spb}(n) \\ \chi_{2spc}(n) \end{bmatrix} + \sigma_2 \times \begin{bmatrix} \{v_{sa}(n) - \chi^T_{sp}(n) \times r_{pa}(n)\} \times r_{pa}(n) \\ \{v_{sb}(n) - \chi^T_{sp}(n) \times r_{pb}(n)\} \times r_{pb}(n) \\ \{v_{sc}(n) - \chi^T_{sp}(n) \times r_{pc}(n)\} \times r_{pc}(n) \end{bmatrix} \end{aligned} \quad (11)$$

The  $\sigma_1, \sigma_2$  is the adaptation constant selected aptly to seize the relevant result, and  $r_{ka}(n)$  is the in-phase unit vector as derived in (5). The combined weight of the convex composition of the two filters for phase ‘a’ is calculated using (12), from the individual weights of the filters.

$$\chi_{spa}(n) = \chi_{1spa}(n) \times \zeta(n) + \chi_{2spa}(n) \times [1 - \zeta(n)] \quad (12)$$

To ensure that the composition is convex, we must find a function of  $\zeta(n)$  that is bounded from zero to one. This property is shared by sigmoid functions, which are also smooth (perfect for derivatives). The sigmoid function plays a crucial role in ensuring a valid convex combination between the two adaptive filters, enabling smooth and stable adaptation. By constraining its value between 0 and 1, it prevents instability by avoiding extreme parameter shifts. This bounded range ensures a gradual and controlled transition between filters, enhancing overall stability. Additionally, it improves performance by allowing dynamic adaptation based on error conditions, effectively optimizing the contribution of each filter within the specified range. The exponential function (sigmoid) further increases the computational burden. However, rapid tracking and precision are the benefits of the aforementioned control algorithm.

### 3.4. Active and reactive loss component estimation

The DC bus voltage  $V_{dc}$  is sensed and then subtracted from the reference DC-bus voltage  $V_{dc}^*$ . It generates the error signal  $V_{de}$  which is passed through the proportional-integral (PI) controller, called ‘DC-

PI'. The PI controller gives the active loss component  $V_{dPI}$  as output, which helps to maintain the DC bus voltage at the rated value and meets the VSC losses modelled at  $m^{th}$  sampling time as (13).

$$v_{dPI}(m) = v_{dPI}(m-1) + k_{pd}(v_{de}(m) - v_{de}(m-1)) + k_{id}(v_{de}(m)) \quad (13)$$

Where,  $k_{pd}$  and  $k_{id}$  are gains of the PI controller. The reference load voltage is calculated, which is 335 V (peak of amplitude of source voltage). To achieve the voltage regulation, the measured load terminal voltage is subtracted from the reference load terminal voltage. The error obtained by taking the difference between reference load terminal voltage and measured load terminal voltage is passed through the PI controller, called 'AC-PI'. The error at the  $m^{th}$  sample instant can be determined as (14).

$$v_{te}(m) = v_t^*(m) - v_t(m) \quad (14)$$

The PI controller gives a reactive loss component  $v_{lPI}$  as output is given by (15).

$$v_{lPI}(m) = v_{lPI}(m-1) + k_{pq}(v_{te}(m) - v_{te}(m-1)) + k_{iq}(v_{te}(m)) \quad (15)$$

The  $k_{pq}$  and  $k_{iq}$  are the proportional as well as integral gain of the ac-PI. The PI controller gains for both the DC-link and AC voltage loops were tuned using a trial-and-error approach in the simulation environment. Initial values were selected based on standard design guidelines, considering system time constants and desired dynamic response. The final gains were chosen once the desired performance was consistently achieved across typical operating conditions.

### 3.5. Generation of reference three-phase load voltage component

The total fundamental active weight component of the load voltage  $V_{Lp}$  is determined by subtracting the DC-PI output (loss component)  $V_{dPI}$  from the averaged active weight component  $\chi_{sp}$ .

$$V_{Lp} = \chi_{sp} - V_{dPI} = V_d - V_{dPI} \quad (16)$$

The active component of the reference load voltage is obtained by multiplying the total fundamental active weight component of the voltage  $V_{Lp}$  with the in-phase unit vectors. This is used for the calculation of the reference load voltage  $v_{labc}^*$  as (17).

$$v_{labc}^* = V_{Lp} \times r_{pabc} \quad (17)$$

The total fundamental reactive weight component of the terminal voltage  $V_{Lq}$  is determined by adding the AC-PI output  $v_{lPI}$  with the averaged reactive weight component  $\chi_{sq}$  as (18).

$$V_{Lq} = V_q + v_{lPI} = \chi_{sq} + v_{lPI} \quad (18)$$

The reactive component of the reference load voltage  $v_{qabc}^*$  is obtained by multiplying the total fundamental reactive weight component of the  $V_{Lp}$  with the quadrature unit vectors  $r_{qabc}$ . This is used for the calculation of reference  $v_{qabc}^*$ .

$$v_{qabc}^* = V_{Lp} \times r_{qpabc} \quad (19)$$

The total reference load voltage  $v_{labc}^*$  is obtained as (20).

$$v_{labc}^* = v_{pabc}^* + v_{qabc}^* \quad (20)$$

## 4. RESULTS AND DISCUSSION

The system is designed with MATLAB/Simulink, with the events created at the source side with the help of a three-phase programmable source. The MATLAB 2016a is employed for the development of the simulation model with a sampling time of 20  $\mu$ s. The voltage sag as well as swell is created at 0.45 sec. to 0.53 sec. and 0.75 sec. to 0.83 sec. respectively. The voltage unbalances and distortions are created at 0.6 sec. to 0.68 sec. and 0.91 sec. to 0.98 sec. respectively. The following subsections describe the overall performance of the

suggested controller with its internal signals, steady state, and dynamic response, along with THD analysis. The parameters used for simulation are provided below:

- System parameters for simulation

Grid voltage with voltage anomalies: 3 phase, 410 V, 50 Hz; load of 10 kVA with 0.82 p.f. (Lagg.); rating of injection-transformer = 11 kVA, 200/200 V; DC-link voltage ( $V_{dc}$ ) = 300 V; DC bus capacitor ( $C_{dc}$ ) = 3300  $\mu$ F; interfacing inductor ( $L_i$ ) = 3 mH; passive ripple filter:  $R_r$  = 6  $\Omega$  and  $C_r$  = 10  $\mu$ F; switching frequency  $f_s$  = 10 kHz, adaptation constant used  $\sigma_1 = \sigma_2 = 0.0001$ .

#### 4.1. Performance of DVR with CLMF-based control algorithm

The internal signals play an important role in investigating the performance of the proposed controller for the operation of the DVR to mitigate all voltage-related anomalies. Figure 3(a) illustrates the internal signals of the proposed controller during voltage sag and unbalance. On the other hand, Figure 3(b) depicts the internal signals of the proposed controller during voltage swell and distortions. Figure 3(a) and Figure 3(b), the subplot (1) indicates the source voltage  $v_{sabc}$  along with all voltage-related power quality issues at the different instants of the period. The average of all three phases of the active and reactive components of weights has been taken. These two parameters i.e.,  $\chi_{sp}$  and  $\chi_{sq}$  are represented in subplots (6) and (7). The average value of the active and reactive components of the source voltage is then passed through the LPF, which gives  $\chi_{sp} = V_d$  and  $\chi_{sq} = V_q$  signals. The output of the DC-PI  $V_{dPI}$  is subtracted from the average of the active component of a source voltage  $V_d$  which gives the load voltage active component  $V_{LP}$ . It is shown in the subplot (8). Similarly, the output of AC-PI  $v_{LP}$  is added with an averaged reactive component of a source voltage  $V_q$  which gives the load voltage active component  $V_{LP}$ . It is shown in the subplot (9). The reference load voltage is depicted in the subplot (10). From the subplot (10), it is observed that the reference load voltage  $v_{labc}^*$  is constant in magnitude and the same as that of the normal condition, irrespective of voltage sag, swell, distortion, and unbalance. It shows the effectiveness of the proposed controller.

#### 4.2. Dynamic and steady state response of DVR with proposed controller

The aggregate DVR performance with a suggested controller is portrayed in Figure 4. Figure 4(a) is dedicated to voltage sag and unbalance, whereas Figure 4(b) represents mitigation during voltage swell and distortions. The subplot (1) of both the figures represents the three-phase source voltage  $v_{sabc}$  with aforementioned events. The maintained load voltage  $v_{labc}$  even during all disturbances is shown in subplot (2) of Figure 4. The voltage inserted by the DVR in all three phases  $v_{inja}$ ,  $v_{injb}$ ,  $v_{injc}$  is represented separately in the subplots (3), (4), and (5). The load terminal voltage  $V_{Lt}$  as well as the DC link voltage  $V_{dc}$  is as shown in subplots (6) and (7), which settle at their reference levels with small variations during supply disturbances. Finally, the load current  $i_{labc}$  is represented in subplot (8). Both Figures 4(a) and 4(b) show that the load voltage is maintained even though there are sag, swell, unbalance, and distortion issues in the supply voltage.

The performance comparison with respect to THD analysis has been presented for conventional LMS, LMF, and CLMF control algorithms in Figure 5(a), which shows both the source voltage and load voltage of algorithms in a graph format. When compared to other algorithms, the source voltage of the CLMF algorithm is 21.78%. The load voltage for CLMF comes out to be only 3.83%.

The performance of the control algorithms after implementing the optimization algorithm for the approximation of PI gains has been assessed using the DC-link voltage response. The DC-bus voltage responses for each of the three control algorithms are shown in Figure 5(b). In this instance, the index parameters for the three control algorithms have been identified as rise time ( $T_r$ ), settle time ( $T_s$ ), and percentage peak overshoot. The rise time ( $T_r$ ) is calculated at 100 % of the final value (i.e. at 300 V). Also, to be noted is the fact that these index parameters were calculated with a 2% tolerance range (294 V-306 V) was used to generate these index values. For the proposed CLMF control algorithm, the rise time, settling time, and % peak overshoot are 0.082 sec., 0.092 sec., and 2.33% respectively, which are indicated by a blue color curve. The LMF control algorithm has a rise time = 0.082 sec., a settle time = 0.1 sec. and % peak overshoot = 3.66% respectively, indicated by the green curve. On the other hand, the rise time, settling time, and % peak overshoot are 0.0797 sec., 0.105 sec., and 5.83% respectively for the LMS algorithm indicated by a red curve. The dynamic performance of the proposed control algorithm, along with LMF and conventional LMS, has been tabulated in Table 1. Although LMS exhibits a marginally faster rise time (0.0797 sec. vs. 0.082 sec.), the claim of 'faster convergence' for CLMF likely pertains to the algorithm's internal convergence behavior -specifically, the speed at which it stabilizes its adaptive coefficients or minimizes the error norm. This metric, distinct from rise time, better reflects the learning efficiency and robustness of CLMF.



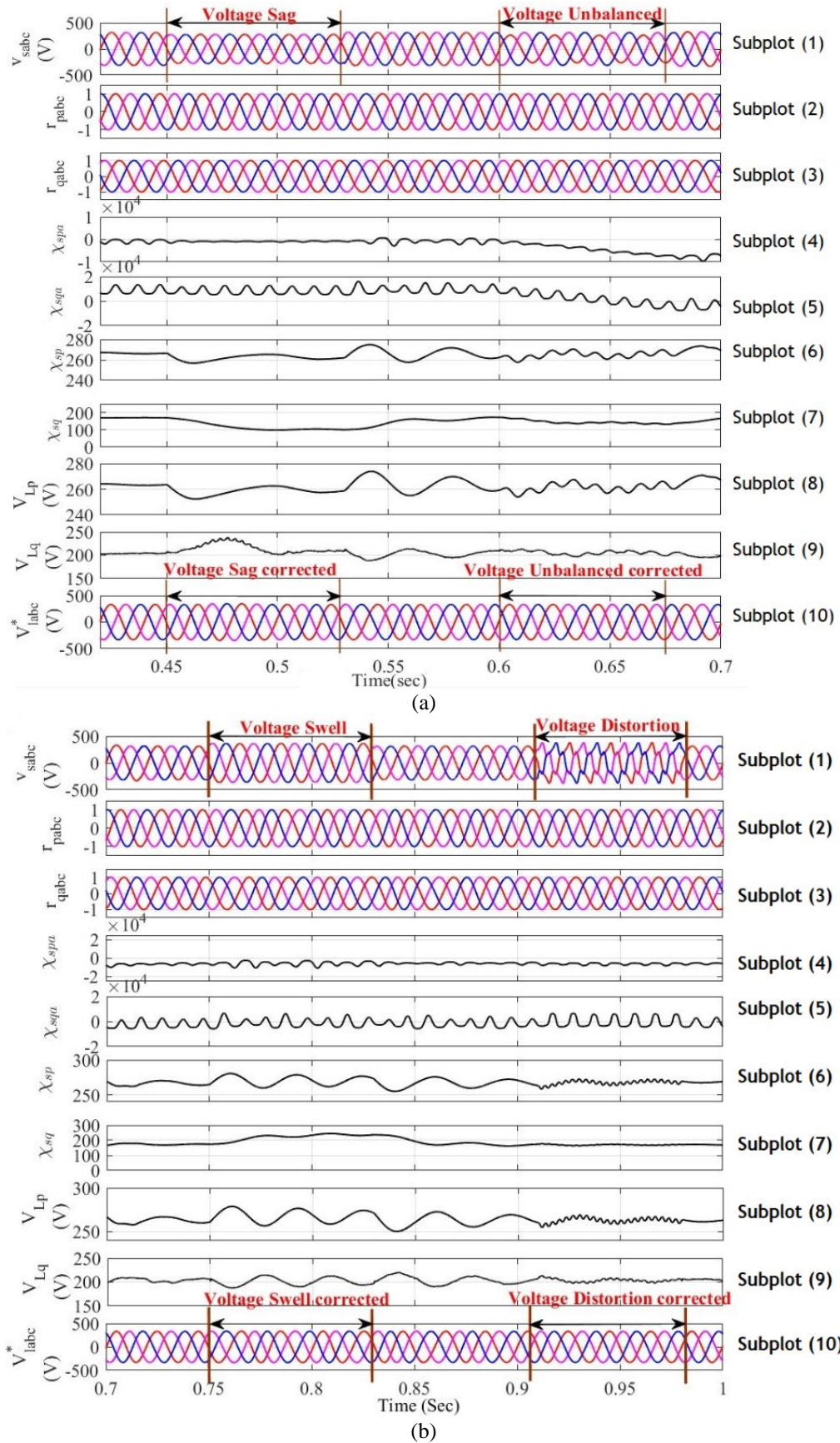


Figure 3. Internal signals of the proposed controller during: (a) voltage sag and voltage unbalance, and (b) voltage swell and voltage distortion



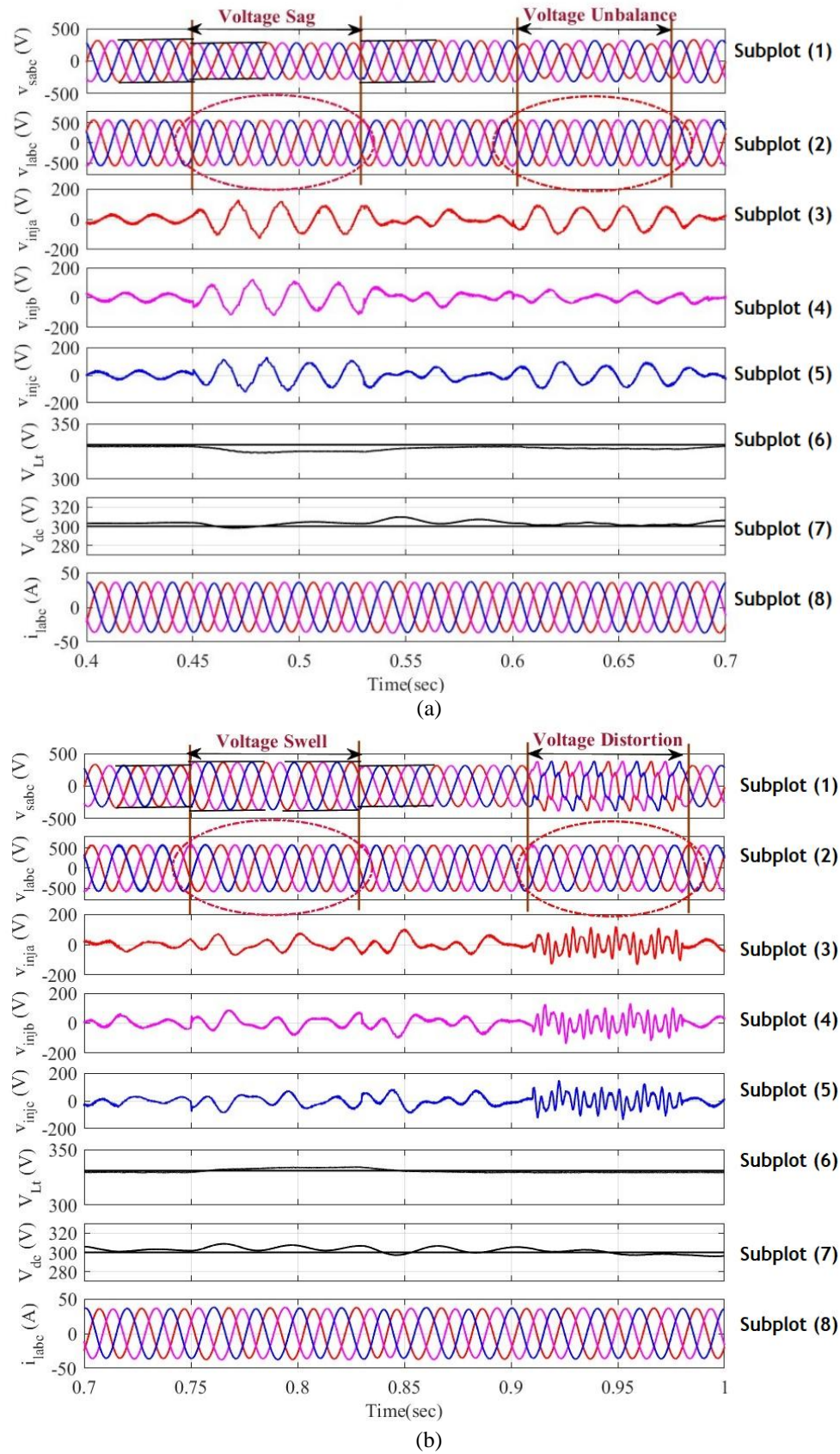


Figure 4. DVR aggregate performance with proposed CLMF algorithm: (a) during voltage sag and unbalance, and (b) during voltage swell and distortion

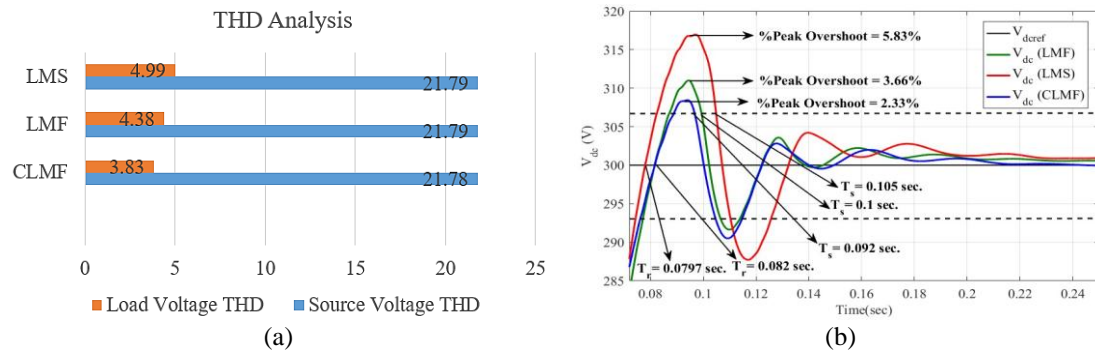


Figure 5. Performance comparison: (a) graphical representation for THD analysis of LMS, LMF, and proposed CLMF control algorithm; and (b) DVR DC-link voltage response by adjusting gains of PI controller with proposed and conventional LMS, LMF control algorithm

Table 1. Comparison of conventional LMS, LMF, and the proposed algorithm

Method	LMS	LMF	CLMF
Type of filter	Adaptive	Adaptive	Adaptive
Rate of convergence	Slower	Fast compared with LMS	Faster compared with LMS
Source voltage THD (%)	21.79	21.79	21.78
Load voltage THD (%)	4.99	4.38	3.83
% Peak overshoot	5.83	3.66 (2% less compared with LMS)	2.33 (3% less compared with LMS)
Rise time ( $T_r$ sec.)	0.0797	0.082	0.082
Settle time ( $T_s$ sec.)	0.105	0.1	0.092

## 5. CONCLUSION

The performance of DVR with an innovative composite least mean fourth (CLMF) control scheme has been discussed. The suggested control algorithm is capable of dynamically responding to voltage-related power quality issues. Additionally, it has been noted that the control algorithm successfully works under distorted and unbalanced signals. In terms of reference voltage extraction and PI gain tuning, the dynamic voltage restorer (DVR) system's performance has significantly improved with the proposed CLMF control algorithm. Results demonstrate that the proposed CLMF-based control scheme gives a better rise time, 0.082 sec., and less settling time, 0.092 sec., respectively, with a peak overshoot of 2.33% compared with conventional LMS and LMF control algorithms. The adaptation constant parameter tuning method is also explained. Because of its adaptive nature, the use of CLMF reduces the computational time and noise in the form of distortions/unbalances and can be easily removed from the signal. According to IEEE 519-2022 std., the load voltage's THD analysis is less than 5%. Thus, it can be concluded that the performance of the developed control algorithm is satisfactory. The limitation of the proposed control algorithm is the difficulty in choosing the mixing parameter.

## FUNDING INFORMATION

Authors did not receive any funding to for this research work.

## AUTHOR CONTRIBUTIONS STATEMENT

This journal uses the Contributor Roles Taxonomy (CRediT) to recognize individual author contributions, reduce authorship disputes, and facilitate collaboration.

Name of Author	C	M	So	Va	Fo	I	R	D	O	E	Vi	Su	P	Fu
Tummala Kranti Kiran	✓	✓	✓	✓	✓	✓		✓	✓	✓			✓	
Balakrishnan Rajagopal		✓				✓		✓	✓	✓	✓	✓		
Yerramilli Butchi Raju	✓		✓	✓		✓			✓		✓		✓	

C : Conceptualization

M : Methodology

So : Software

Va : Validation

Fo : Formal analysis

I : Investigation

R : Resources

D : Data Curation

O : Writing - Original Draft

E : Writing - Review & Editing

Vi : Visualization

Su : Supervision

P : Project administration

Fu : Funding acquisition

## CONFLICT OF INTEREST STATEMENT

Authors state no conflict of interest.

## DATA AVAILABILITY

Data availability is not applicable to this paper as no new data were created or analyzed in this study.




## REFERENCES

- [1] M. Farhadi-Kangarlou, E. Babaei, and F. Blaabjerg, "A comprehensive review of dynamic voltage restorers," *International Journal of Electrical Power and Energy Systems*, vol. 92, pp. 136–155, 2017, doi: 10.1016/j.ijepes.2017.04.013.
- [2] M. Mansoor, N. Mariun, A. Toudeshki, N. I. Abdul Wahab, A. U. Mian, and M. Hojabri, "Innovating problem solving in power quality devices: A survey based on dynamic voltage restorer case (DVR)," *Renewable and Sustainable Energy Reviews*, vol. 70, pp. 1207–1216, 2017, doi: 10.1016/j.rser.2016.12.022.
- [3] S. Padmanaban, C. Sharmela, J. B. Holm-Nielsen, and P. Sivaraman, *Power quality in modern power systems*. Elsevier, 2021, doi: 10.1016/B978-0-12-823346-7.01001-X.
- [4] S. Abdul Rahman and E. Dagnew, "Voltage sag compensation using direct converter based DVR by modulating the error signal," *Indonesian Journal of Electrical Engineering and Computer Science*, vol. 19, no. 2, pp. 608–616, 2020, doi: 10.11591/ijeecs.v19.i2.pp608-616.
- [5] IEEE, "IEEE recommended practice for evaluating electric power system compatibility with electronic process equipment." IEEE Std 1346-1998, Piscataway, NJ, USA, May 05, 1998, doi: 10.1109/IEEESTD.1998.87816.
- [6] C. Tu, Q. Guo, F. Jiang, H. Wang, and Z. Shuai, "A comprehensive study to mitigate voltage sags and phase jumps using a dynamic voltage restorer," *IEEE Journal of Emerging and Selected Topics in Power Electronics*, vol. 8, no. 2, pp. 1490–1502, 2020, doi: 10.1109/JESTPE.2019.2914308.
- [7] M. H. J. Bollen, "Voltage sags: effects, mitigation and prediction," *Power Engineering Journal*, vol. 10, no. 3, pp. 129–135, 1996, doi: 10.1049/pe:19960304.
- [8] S. Hasan, K. Muttaqi, D. Sutanto, and M. A. Rahman, "A novel dual slope delta modulation technique for a current source inverter based dynamic voltage restorer for mitigation of voltage sags," *IEEE Transactions on Industry Applications*, vol. 57, no. 5, pp. 5437–5447, Sep. 2021, doi: 10.1109/TIA.2021.3089984.
- [9] K. Y. Priya, A. Eswari, and B. Balaji, "Implementation of PLL based artificial neural network controlled dynamic voltage restorer during fault and non-linear load," in *2021 22nd International Conference on Smart Electronics and Communication (ICOSEC)*, IEEE, Oct. 2021, pp. 1412–1417, doi: 10.1109/ICOSEC51865.2021.9591975.
- [10] R. H. Yang *et al.*, "A battery-energy-storage-based DC dynamic voltage restorer for DC renewable power protection," *IEEE Transactions on Sustainable Energy*, vol. 13, no. 3, pp. 1707–1721, Jul. 2022, doi: 10.1109/TSTE.2022.3164795.
- [11] D. G. A. Krishna and A. Karthikeyan, "Design and analysis of frequency adaptive CDSC-PLL for dynamic voltage restorer during adverse grid conditions," in *2020 IEEE International Conference on Power Electronics, Smart Grid and Renewable Energy (PESGRE2020)*, IEEE, Jan. 2020, pp. 1–5, doi: 10.1109/PESGRE45664.2020.9070625.
- [12] Z. Elkady, N. Abdel-Rahim, A. Mansour, and F. Bendary, "Voltage sag/swell detection based on decoupled stationary reference frame PLL in DVR," in *2021 22nd International Middle East Power Systems Conference (MEPCON)*, IEEE, Dec. 2021, pp. 678–682, doi: 10.1109/MEPCON50283.2021.9686301.
- [13] M. Bajaj and A. kumar Singh, "Designing of a solar energy based single phase dynamic voltage restorer using fuzzy logic controlled novel boost inverter," in *2020 IEEE 9th Power India International Conference (PIICON)*, IEEE, Feb. 2020, pp. 1–6, doi: 10.1109/PIICON49524.2020.9112965.
- [14] H. Komurcugil, S. Bayhan, N. Guler, and S. Biricik, "Super twisting sliding-mode control strategy for three-level dynamic voltage restorers," in *2021 IEEE 30th International Symposium on Industrial Electronics (ISIE)*, IEEE, Jun. 2021, pp. 1–6, doi: 10.1109/ISIE45552.2021.9576474.
- [15] J. Xiu, X. Guangye, M. Xiangping, and D. Guilin, "Voltage sag detection method based on dq transform and complex wavelet transform," in *2021 IEEE International Conference on Electrical Engineering and Mechatronics Technology (ICEEMT)*, IEEE, Jul. 2021, pp. 429–434, doi: 10.1109/ICEEMT52412.2021.9602691.
- [16] A. Khergade, R. Satputaley, and S. K. Patro, "Investigation of voltage sags effects on ASD and mitigation using ESRF theory-based DVR," *IEEE Transactions on Power Delivery*, vol. 36, no. 6, pp. 3752–3764, Dec. 2021, doi: 10.1109/TPWRD.2020.3048838.
- [17] H. M. M. Alhaj, N. M. Nor, V. S. Asirvadam, and M. F. Abdullah, "Power system harmonics estimation using LMS, LMF and LMS/LMF," *2014 5th International Conference on Intelligent and Advanced Systems: Technological Convergence for Sustainable Future, ICIAS 2014 - Proceedings*, pp. 1–5, 2014, doi: 10.1109/ICIAS.2014.6869521.
- [18] R. K. Agarwal, I. Hussain, and B. Singh, "LMF-based control algorithm for single stage three-phase grid integrated solar PV system," *IEEE Transactions on Sustainable Energy*, vol. 7, no. 4, pp. 1379–1387, Oct. 2016, doi: 10.1109/TSTE.2016.2553181.
- [19] M. Srinivas, I. Hussain, and B. Singh, "Combined LMS-LMF-based control algorithm of DSTATCOM for power quality enhancement in distribution system," *IEEE Transactions on Industrial Electronics*, vol. 63, no. 7, pp. 4160–4169, 2016, doi: 10.1109/TIE.2016.2532278.
- [20] T. A. Naidu, S. R. Arya, and R. Maurya, "Control of DVR using variable step-size griffith's LMS with optimized tuning of proportional integrator gains," *1st International Conference on Power Electronics Applications and Technology in Present Energy Scenario, PETPES 2019 - Proceedings*, pp. 1–7, 2019, doi: 10.1109/PETPES47060.2019.9004017.
- [21] T. A. Naidu, A. Al-Durra, T. H. M. El-Fouly, and H. Zeineldin, "Optimization based variable learning factor least mean square algorithm to control DVR in infected grid systems," in *2020 IEEE International Conference on Power Electronics, Drives and Energy Systems (PEDES)*, IEEE, Dec. 2020, pp. 1–6, doi: 10.1109/PEDES49360.2020.9379450.
- [22] E. Walach and B. Widrow, "The least mean fourth (LMF) adaptive algorithm and its family," *IEEE Transactions on Information Theory*, vol. 30, no. 2, pp. 275–283, 1984, doi: 10.1109/TIT.1984.1056886.
- [23] G. Gui, W. Peng, and F. Adachi, "Adaptive system identification using robust LMS/F algorithm," *International Journal of Communication Systems*, vol. 27, no. 11, pp. 2956–2963, 2014, doi: 10.1002/dac.2517.




- [24] P. I. Hubscher, J. C. M. Bermudez, and V. H. Nascimento, "A mean-square stability analysis of the least mean fourth adaptive algorithm," *IEEE Transactions on Signal Processing*, vol. 55, no. 8, pp. 4018–4028, 2007, doi: 10.1109/TSP.2007.894423.
- [25] V. H. Nascimento and J. C. M. Bermudez, "When is the least-mean fourth algorithm mean-square stable?," *ICASSP, IEEE International Conference on Acoustics, Speech and Signal Processing - Proceedings*, vol. 4, pp. iv–341, 2005, doi: 10.1109/ICASSP.2005.1416015.

## BIOGRAPHIES OF AUTHORS






**Tummala Kranti Kiran**    is an Assistant Professor in the Department of Electrical Engineering at Sir C R Reddy College of Engineering, Eluru, Andhra Pradesh, India. He received his B.Tech. and M.Tech. degrees in Electrical Engineering in 2003 and 2006, respectively. He has been working as an assistant professor since 2007. He is, at present, the External Research Scholar of Annamalai University, Annamalaiagar, Tamil Nadu, India. His research interests include power systems, power electronics, motor drives, and renewable energy. He can be contacted at email: krantikiran.tummala@gmail.com.



**Dr. Balakrishnan Rajagopal**    is an Associate Professor in the Department of Electrical Engineering at Annamalai University, Annamalaiagar, Tamil Nadu, India. He received his B.E., M.E., and Ph.D. degrees in electrical engineering. He has been working as an associate professor since 2001. He published 10 papers in international journals. His research interests include electrical machines, power electronics, IoT-based systems, renewable energy, high voltage engineering, and power systems. He can be contacted at email: ba\_raj7278@rediffmail.com.



**Dr. Yerramilli Butchi Raju**    is a Professor in the Department of Electrical Engineering at Sir C R Reddy College of Engineering, Eluru, Andhra Pradesh, India. He received his B.Tech, M.Tech., and Ph.D. degrees in Electrical Engineering in 1999, 2004, and 2012, respectively. He has been working as a professor since 2016. He published 15 papers in International Journals. His research interests include power system dynamics, power electronics, IoT-based systems, and renewable energy. He can be contacted at email: butchiraju.y@gmail.com.